The Astronomical Journal, 130:1345–1357, 2005 October

THE OPTICAL–INFRARED COLORS OF CORALS QSOs: SEARCHING FOR DUST REDDENING ASSOCIATED WITH HIGH-REDSHIFT DAMPED Lyα SYSTEMS[1]

Sara L. Ellison
Department of Physics and Astronomy, University of Victoria, Elliott Building, 3800 Finnerty Road, Victoria, BC V8P 1A1, Canada; sarae@uvic.ca

Patrick B. Hall
Department of Physics and Astronomy, York University, 4700 Keele Street, Toronto, ON M3J 1P3, Canada; phall@yorku.ca

and

Paulina Lira
Departamento de Astronomía, Universidad de Chile, Casilla 36-D, Santiago, Chile; plira@das.uchile.cl
Received 2005 February 28; accepted 2005 June 26

ABSTRACT

The presence of dust in quasar absorbers, such as damped Lyα (DLA) systems, may cause the background QSO to appear reddened. We investigate the extent of this potential reddening by comparing the optical-to-infrared colors of QSOs with and without intervening absorbers. Our QSO sample is based on the Complete Optical and Radio Absorption Line System (CORALS) survey of Ellison and coworkers. The CORALS data set consists of 66 radio-selected QSOs at $z_{\rm em} \geq 2.2$ with complete optical identifications. We have obtained near-simultaneous *B*- and *K*-band magnitudes for a subset of the CORALS sample and supplemented our observations with further measurements published in the literature. In total, we have $B - K$ colors for 42 of the 66 QSOs, of which 14 have intervening DLA systems. To account for redshift-related color changes, the $B - K$ colors are normalized using the Sloan Digital Sky Survey QSO composite. The mean normalized $B - K$ color of the DLA subsample is +0.12, whereas the mean for the no-DLA sample is −0.10; both distributions have rms scatters of ∼0.5. Neither a Student's *t*-test nor a Kolmogorov-Smirnov test indicate that there is any significant difference between the two color distributions. Based on simulations that redden the colors of QSOs with intervening DLA systems, we determine a reddening limit that corresponds to $E(B - V) < 0.04$ (SMC-like extinction) at 99% confidence (3 σ), assuming that $E(B - V)$ is the same for all DLA systems. Finally, we do not find any general correlation between absorber properties (such as [Fe/Zn] or neutral hydrogen column density) and $B - K$ color. The two reddest QSOs with DLA systems in our sample have H I column densities that differ from each other by an order of magnitude and moderate gas-to-dust ratios as inferred from chemical abundances. One of these two QSOs shows evidence for strong associated absorption from X-ray observations, an alternative explanation for its very red color. We conclude that the presence of intervening galaxies causes a minimal reddening of the background QSO.

Key words: dust, extinction — galaxies: high-redshift — ISM: general — quasars: absorption lines

Online material: color figures, machine-readable table

1. INTRODUCTION

1.1. *Red Quasars*

Although quasars are usually regarded as objects that are characterized by an ultraviolet (UV) excess, the existence of red QSOs has been known for more than two decades (e.g., Smith & Spinrad 1980; Bregman et al. 1981; Stein & Sitko 1984). Despite their long history, red QSOs have continued to attract much interest in the literature, most notably the ongoing debate to identify the primary cause of their extreme optical–infrared (IR) colors. Probably the most popular explanation for red QSOs is extinction due to dust at the systemic redshift, a conclusion that is gaining substantial support from the current generation of large QSO surveys (e.g., Richards et al. 2003; Hopkins et al. 2004; Glikman et al. 2004; White et al. 2003). There are also convincing examples of individual QSOs that appear to have been highly reddened due to local (to the QSO) dust (e.g., Rawlings et al. 1995; Gregg et al. 2000; Stern et al. 2003). If dust is indeed a common ingredient in QSOs, the corollary is that samples based on optically selected sources could potentially miss the reddened population, whereas radio-selected quasars would represent a more complete sample (e.g., Webster et al. 1995; Barkhouse & Hall 2001). Indeed, Webster et al. (1995) have claimed that up to 80% of QSOs may be hidden from the eyes of optical surveys due to dust extinction.

However, some observations do not support the hypothesis of dust local to the QSO as the cause of reddening. For example, millimeter observations (Drinkwater et al. 1996) of 11 of the reddest Webster et al. (1995) sources failed to detect CO, which argues against the presence of host galaxy dust in these cases. Other possible sources of QSO reddening include the effect of host galaxy starlight and synchrotron radiation (Francis et al. 2000, hereafter FWW00; Whiting et al. 2001; Benn et al. 1998).

1.2. *Dust Reddening Associated with Intervening Galaxies*

One factor that could have a significant impact on reddening QSO light that remains relatively unexplored is the presence of intervening dust located in foreground galaxies. The identification of a handful of red lensed QSOs lends credibility to this

[1] These data were obtained from the NTT on La Silla (ESO program 072.A-0014 [A, B, C, D]).

scenario, in which dust in the lensing galaxy reddens the background source (e.g., Gregg et al. 2000; Falco et al. 1999; Wucknitz et al. 2003). The issue of dusty intervening galaxies is of interest, not only in order to assess its contribution to the red QSO population, but it is also of crucial importance for the study of quasar absorption lines. Quasar absorbers, such as the damped Lyα (DLA) systems that correspond to the signatures of high-redshift galaxies imprinted on the continuum of a background QSO, represent one of our best tools for studying the early galaxy population. Previous surveys for DLA systems have almost universally relied on large optical databases of QSOs to find intervening absorbers. Since only relatively bright, optically selected QSOs have been used to identify DLA systems, there has been widespread concern that dusty intervening galaxies may obscure the background QSO so that it drops below the survey magnitude limit. Such a selection effect would result in a biased view of high-redshift galaxies. This general concern has been quantified in a number of theoretical works that have attempted to estimate the amount of reddening that a QSO may suffer and consequently what fraction of the DLA population, and its contribution toward the cosmic gas and metals budget, may have been overlooked (e.g., Fall & Pei 1993; Pei & Fall 1995; Pei et al. 1999; Churches et al. 2004; Vladilo & Péroux 2005). However, until recently there had been little observational progress in quantifying the number of missed DLA systems due to extinction effects.

The first systematic program to quantify dust bias was undertaken by Ellison et al. (2001) by searching for DLA systems in an optically complete radio-selected sample of QSOs. The Complete Optical and Radio Absorption Line System (CORALS) survey was based on a homogeneous sample of 66 radio-selected, flat-spectrum QSOs taken from the Parkes catalog, complete down to 0.25 Jy. Extensive optical follow-up observations resulted in identifications for *all* sources. Therefore, subsequent spectroscopic searches for DLA systems were based on a complete sample, ideal for determining the extent to which intervening galaxies obscure background QSOs. Ellison et al. (2001) determined that the neutral gas mass density of DLA systems ($\Omega_{\rm DLA}$) may have been previously underestimated by at most a factor of $\sim$2. However, this work also found tentative evidence that $\Omega_{\rm DLA}$ and $n(z)$ (the DLA number density) may be underestimated for bright QSO samples with magnitude limits $B \lesssim 19.5$. Ellison et al. (2004) revisited this issue and suggested that this could be understood in terms of an Eddington bias if the optical luminosity function deviates from a simple power law. To extend the original CORALS sample to lower redshifts, Ellison et al. (2004) studied Mg II absorption systems in an analogous radio-selected QSO sample. The main conclusion of that work was that the number density of intervening systems selected via Mg II absorption in the range $0.6 < z < 1.7$ is in excellent agreement with magnitude-limited samples (e.g., Nestor et al. 2005). Most recently, Akerman et al. (2005) have measured the metal abundances of $z > 1.8$ CORALS DLA systems and found that the weighted mean metallicity based on zinc (an undepleted proxy for Fe) is only marginally higher (but consistent within the error bars) than previous samples.

Although the results from CORALS indicate that magnitude-limited surveys (at least those complete to $B \sim 19$) have not missed a significant fraction of the gas or metals budget, this is not to say that DLA systems are dust-free. In fact, it has been known for over a decade, based on the ratios of refractory and nonrefractory elements, that dust is present in DLA systems (Meyer & Roth 1990; Meyer & York 1992; Pettini et al. 1994, 1997). Understanding the level of extinction caused by this dust has so far yielded conflicting results. For example, Fall et al. (1989) and Pei et al. (1991) found a significant difference between the spectral indices of QSOs with intervening DLA systems and a control sample. However, this result has not been reproduced with larger, homogeneous QSO samples. Currently, the most stringent limit for reddening due to intervening DLA systems has been obtained from fitting spectral indices to $\sim$1450 QSOs from the Sloan Digital Sky Survey (SDSS): $E(B-V) < 0.02$ for SMC-like extinction (Murphy & Liske 2004). Despite this sensitive limit, studies of spectral indices suffer from two drawbacks: they use limited wavelength coverage in the optical regime and have not yet been conducted on unbiased samples (i.e., they were taken from magnitude-limited surveys).

1.3. *Optical–Infrared Colors and Extinction Curves*

In this work, we take a different approach to studying the effect of dust extinction from intervening DLA systems by using optical–IR QSO colors to search for a reddening signature. This technique has the advantage of using a wide wavelength baseline, from the observed frame B to K bands, over which to detect the effect of extinction. Moreover, by studying QSOs from the CORALS survey, we have a sample that is optically complete and in which all of the intervening high-redshift DLA systems have already been identified and metallicities measured.

The observed reddening obviously depends largely on the assumed extinction law, although the QSO and galaxy (i.e., dust) redshift also play a part (as we demonstrate below). Despite its ubiquity in astrophysical environments, the properties of dust remain relatively poorly understood (see reviews by Mathis [1990] and Draine [2003]), and reliable empirical extinction data are available for only the Milky Way (MW) and Magellanic Clouds. In particular, data are sparse in the far-ultraviolet (FUV; Hutchings & Giasson 2001), and below the Lyman limit there is simply no flux with which to work. FUV wavelengths are particularly important for the present work, which considers the optical–IR colors of high-redshift QSOs. The most often used parameterization of Galactic extinction is that of Cardelli et al. (1989, hereafter CCM89). The advantage of the CCM89 formulae is that $\xi(\lambda) = A_\lambda/A_V$ can be calculated for any value of R_V.[2] Another popular parameterization of Galactic extinction is that of Pei (1992), although this is for a fixed value of $R_V = 3.08$. A comparison of these two extinction-law fits is shown in Figure 1, with an $R_V = 3.08$ for the CCM89 law in order to match the Pei (1992) curve. It can be seen that at IR and optical wavelengths, the two curves are in close agreement. However, in the FUV ($\lambda < 1200$ Å) the curves diverge; this is purely due to extrapolation of the different fitting functions into a regime in which no data are available. Whereas an extrapolation of the Pei (1992) parameterization leads to a flattening of $\xi(\lambda)$, the CCM89 curve rises quickly at FUV wavelengths. In Figure 1 we also show the extinction curves of the SMC and LMC as fitted by Pei (1992), again extrapolated to the FUV using the published fitting functions.

We illustrate the expected reddening due to intervening dust in Figures 2–4. In each figure, we plot the theoretical reddening (as measured by a change in the $B-K$ color) of a QSO at $z_{\rm em} = 3$ as a function of $E(B-V)$. Since the color change depends on the redshift of the intervening dust, four different lines are plotted for dust, at $z_{\rm dust} = 2.0$, 2.3, 2.6, and 2.9. The reddening induced by the two Galactic extinction curves is quite similar, although a CCM89 law produces slightly redder colors due to the rapid rise of $\xi(\lambda)$ in the FUV. Reddening is most severe for SMC-type dust and could be even more extreme if the true extinction law

[2] In the usual notation, $R_V = A_V/E(B-V)$, i.e., the total-to-selective extinction.

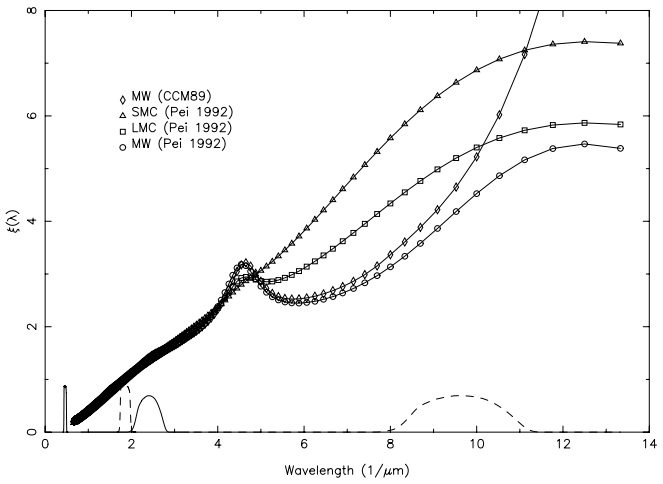

FIG. 1.—Extinction curves for the parameterizations of Pei (1992) and CCM89. Assumed R_V values are 2.93 (SMC), 3.16 (LMC), and 3.08 (MW). There were no data available at wavelengths $\leq$1000 Å; hence, the divergence in the FUV for the Galactic curves represents an extrapolation of the fitting functions. Filter transmission curves along the base of the plot illustrate what rest wavelengths correspond to the B and K_s bands for $z = 0$ (*solid line*) and $z = 3$ (*dashed line*). [*See the electronic edition of the Journal for a color version of this figure*.]

continues to rise at FUV wavelengths. That is, the parameterization of SMC dust by Pei (1992) may be considered conservative.

2. OBSERVATIONS AND DATA REDUCTION

Since flat-spectrum radio-loud QSOs (RLQs) are highly variable, it is important to obtain optical and IR data from near-simultaneous epochs (e.g., FWW00). We achieved this by using the optical (SuSI2) and IR (SofI) imagers on the New Technology Telescope (NTT) at La Silla Observatory. Since both instruments are mounted on the same Nasmyth platform, the overhead incurred by switching between them is typically only about 2 minutes, depending on the source position relative to the zenith. Our strategy was therefore to observe a sequence of QSOs in the optical and then change to the IR. Optical and IR photometric standard stars were observed throughout the night at air masses up to 1.8.

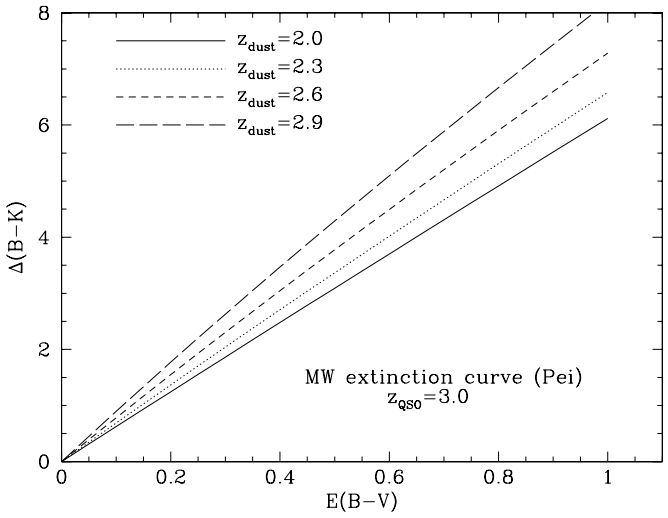

FIG. 2.—Theoretical reddening of a $z_{em} = 3.0$ QSO with an intervening absorber at $z_{abs} = 2.0$, 2.3, 2.6, and 2.9. We assume a Galactic extinction curve based on the parameterization of Pei (1992). [*See the electronic edition of the Journal for a color version of this figure*.]

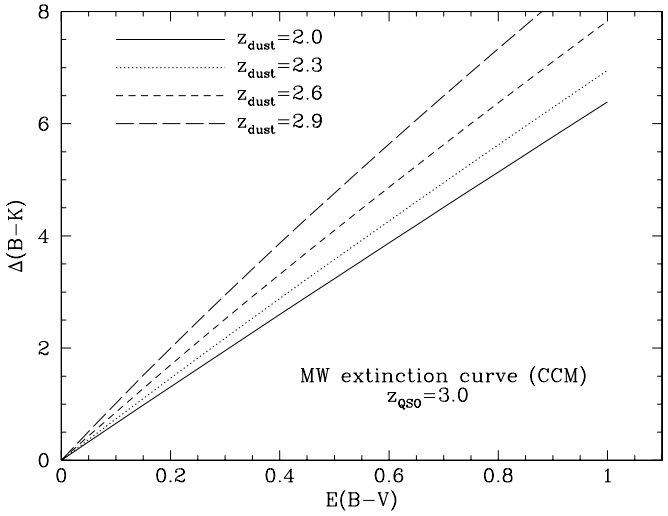

FIG. 3.—Same as Fig. 2, but based on the parameterization of CCM89 with $R_V = 3.08$. [*See the electronic edition of the Journal for a color version of this figure*.]

Our data were obtained during two runs in 2003 October and 2004 March. The 2004 March run experienced excellent conditions: photometric transparency and typical seeing $\sim$0.″6. The earlier 2003 October run suffered from somewhat poorer seeing ($\sim$1″), and the end of the last night (during which only SofI was used) was not photometric.

2.1. *Optical Imaging*

In addition to B-band images, we obtained supplemental V-band images for most QSOs with redshifts $z_{em} > 3.0$. Typical exposure times in the B and V bands ranged from 10 to 200 s (see Table 1); the total integration was divided between two exposures with a spatial offset of a few hundred pixels between exposures. We used SuSI2 in 2×2 binning mode, which yielded a pixel scale of 0.″16 pixel^{-1}. Standard IRAF procedures were used for the reduction of the optical data; a bias was constructed from a median combination of five frames, and the overscan was fitted and subtracted interactively. The initial flat-fielding was executed using dome flats to correct pixel-to-pixel variations, followed by an illumination correction of large-scale variations constructed from a

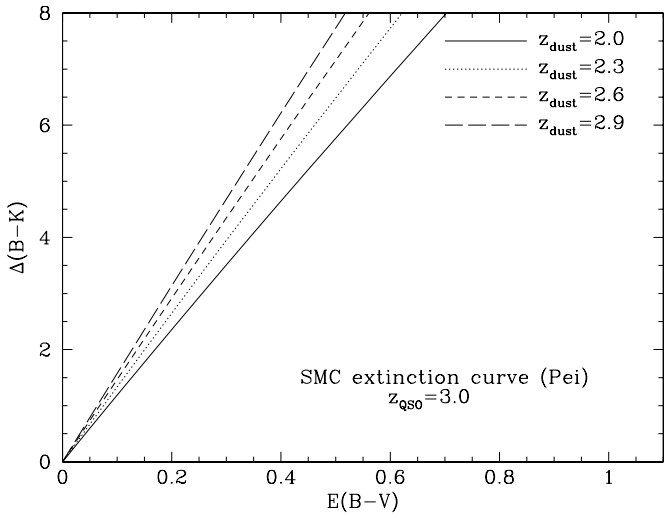

FIG. 4.—Theoretical reddening of a $z_{em} = 3.0$ QSO with an intervening absorber at $z_{abs} = 2.0$, 2.3, 2.6, and 2.9. We assume an SMC extinction curve based on the parameterization of Pei (1992). [*See the electronic edition of the Journal for a color version of this figure*.]

TABLE 1
Target List and Observing Journal

QSO	z_{em}	Observing Run	Integration Time SofI (s)	Integration Time SuSI2 (s)	SuSI2 Filter
B0113−283	2.555	2003 Oct	1800	200	*B*
B0122−005	2.280	2003 Oct	300	...	...
B0244−128	2.201	2003 Oct	300	40	*B*
B0256−393	3.449	2003 Oct	4320	360	*V*
B0325−222	2.220	2003 Oct	300	150	*B*
B0329−255	2.685	2003 Oct	200	40	*B*
B0335−122	3.442	2003 Oct	4500	360	*V*
B0347−211	2.944	2003 Oct	...	800	*B*
B0405−331	2.570	2003 Oct	600	60	*B*
B0420+022	2.277	2003 Oct	800	100	*B*
B0422−389	2.346	2003 Oct	300	40	*B*
B0432−440	2.649	2003 Oct	800	100	*B*
B0434−188	2.702	2003 Oct	1800	200	*B*
B0438−436	2.863	2003 Oct	800	100	*B*
B0451−282	2.560	2003 Oct	300	60	*B*
B0458−020	2.286	2003 Oct	1200	200	*B*
B0528−250	2.765	2003 Oct	300	60	*B*
B0537−286	3.110	2004 Mar	1800	200	*B*
				200	*V*
B0610−436	3.461	2003 Oct	300	60	*V*
B0919−260	2.300	2004 Mar	300	60	*B*
B0933−333	2.906	2004 Mar	1800	200	*B*
				200	*V*
B1010−427	2.954	2004 Mar	800	20	*B*
				20	*V*
B1055−301	2.523	2004 Mar	800	100	*B*
B1136−156	2.625	2004 Mar	800	200	*B*
B1147−192	2.489	2004 Mar	4500	360	*B*
B1149−084	2.370	2004 Mar	1800	200	*B*
B1228−113	3.528	2004 Mar	4920	800	*B*
				800	*V*
B1228−310	2.276	2004 Mar	1800	200	*B*
B1230−101	2.394	2004 Mar	1800	200	*B*
B1256−243	2.263	2004 Mar	800	100	*B*
B1318−263	2.027	2004 Mar	4500	800	*B*
B1351−018	3.710	2004 Mar	...	800	*B*
B1354−107	3.006	2004 Mar	300	60	*B*
				60	*V*
B1402−012	2.518	2004 Mar	300	20	*B*
B1418−064	3.689	2004 Mar	4500	360	*B*
				360	*V*
B2311−373	2.476	2003 Oct	300	40	*B*

super–sky flat. Instrumental magnitudes were determined for each night using IRAF's *qphot* package with between 20 and 40 standard stars taken from Landolt (1992). The photometric solution (zero points and extinction coefficients) for each night in the *B* and *V* bands was determined by a least-squares fit to the data. The zero points determined in this way indicated that conditions were photometric throughout the optical observations. The rms error in the photometric solution was 0.04 mag in the *V* and *B* bands for the 2003 October run and 0.04 and 0.07 mag for the *V* and *B* bands, respectively, in 2004 March. The final quoted *B*- and *V*-band errors in Table 2 include the uncertainty in the fit of the photometric solution and photon statistics added in quadrature.

2.2. *Infrared Imaging*

Each SofI K_s-band integration consisted of a series of coadded 10 s exposures with a random offset within a 40″ jitter box between each exposure. Total on-source integration times ranged between 100 and 5400 s (see Table 1). IR data reduction was carried out using Pat Hall's Infrared Imaging Reduction Software (PHIIRS), which incorporates many standard IRAF routines. We did not follow the usual procedure of obtaining dark frames due to the nonlinearity of dark current with incident flux. Instead, we used the PHIIRS task *irsky* to combine individual dithered exposures to simultaneously remove dark current and sky. We used 4–6 frames to construct the sky image for each science exposure; fewer frames were used when the telescope was observing at low air mass, since pupil ghosts produce more severe artifacts when the pupil plane rotates more quickly. These ghosts remained in a few of the final science images but do not affect the central part of the array in which the QSO is located. Flat-fielding was done using SofI's special dome flats and custom-written reduction script available from the NTT Web site.[3] Registration of the dithered images and median co-addition were done with the PHIIRS routines *irshift* and *ircoadd*, scaling the

[3] See http://www.ls.eso.org/lasilla/sciops/ntt/sofi/reduction/flat_fielding.html.

TABLE 2
CORALS QSO Magnitudes

QSO	z_{em}	b_J	B	V	K_s	References
B0017−307	2.666	20.0	...	...	...	...
B0039−407	2.478	19.7	...	...	...	...
B0104−275	2.492	19.3	...	...	...	...
B0113−283	2.555	19.6	19.64 ± 0.04	...	17.32 ± 0.15	1
B0122−005	2.280	17.9	...	...	15.75 ± 0.03	1
B0244−128	2.201	18.4	18.21 ± 0.04	...	15.13 ± 0.10	1
B0256−393	3.449	20.6	...	19.32 ± 0.04	16.78 ± 0.04	1
B0325−222	2.220	19.0	19.37 ± 0.04	...	16.44 ± 0.04	1
B0329−255	2.685	17.6	18.11 ± 0.04	...	16.00 ± 0.15	1
B0335−122	3.442	20.6	...	20.11 ± 0.04	17.51 ± 0.18	1
B0347−211	2.944	20.5	20.89 ± 0.04	...	...	1
B0405−331	2.570	19.1	19.41 ± 0.04	...	16.28 ± 0.04	1
B0420+022	2.277	19.7	19.17 ± 0.04	...	16.37 ± 0.04	1
B0422−389	2.346	18.4	19.11 ± 0.04	...	16.60 ± 0.13	1
B0432−440	2.649	19.9	19.81 ± 0.04	...	17.37 ± 0.04	1
B0434−188	2.702	18.8	19.25 ± 0.04	...	16.24 ± 0.07	1
B0438−436	2.863	19.4	20.68 ± 0.04	...	16.09 ± 0.03	1
B0451−282	2.560	18.0	18.22 ± 0.04	...	15.35 ± 0.03	1
B0458−020	2.286	...	19.33 ± 0.04	...	15.32 ± 0.03	1
B0528−250	2.765	18.1	18.16 ± 0.04	...	15.46 ± 0.03	1
B0537−286	3.110	20.0	19.84 ± 0.07	19.06 ± 0.04	16.16 ± 0.03	1
B0601−172	2.711	...	...	...	...	...
B0610−436	3.461	18.5	...	18.85 ± 0.04	14.43 ± 0.03	1
B0819−032	2.352	...	...	...	...	...
B0834−201	2.752	...	...	...	...	...
B0913+003	3.074	20.9	...	...	...	...
B0919−260	2.300	...	18.05 ± 0.07	...	15.04 ± 0.03	1
B0933−333	2.906	...	19.72 ± 0.07	19.39 ± 0.04	16.71 ± 0.04	1
B1010−427	2.954	...	17.25 ± 0.07	16.61 ± 0.03	15.31 ± 0.03	1
B1055−301	2.523	19.3	19.36 ± 0.07	...	16.35 ± 0.03	1
B1136−156	2.625	19.1	19.31 ± 0.07	...	16.26 ± 0.03	1
B1147−192	2.489	20.3	20.38 ± 0.07	...	17.08 ± 0.04	1
B1149−084	2.370	20.0	19.70 ± 0.07	...	16.52 ± 0.04	1
B1228−113	3.528	21.5	20.85 ± 0.07	19.48 ± 0.04	16.66 ± 0.03	1
B1228−310	2.276	19.8	19.36 ± 0.07	...	16.79 ± 0.04	1
B1230−101	2.394	19.6	19.73 ± 0.07	...	16.99 ± 0.04	1
B1251−407	4.464	...	...	...	...	...
B1256−243	2.263	19.4	19.45 ± 0.07	...	16.36 ± 0.03	1
B1318−263	2.027	21.3	21.37 ± 0.07	...	17.57 ± 0.03	1
B1351−018	3.710	21.5	21.00 ± 0.07	...	...	1
B1354−107	3.006	18.4	19.00 ± 0.07	18.15 ± 0.04	15.70 ± 0.03	1
B1402−012	2.518	18.0	18.50 ± 0.07	...	15.63 ± 0.03	1
B1406−267	2.430	...	...	...	...	...
B1418−064	3.689	20.5	20.42 ± 0.07	18.97 ± 0.04	16.58 ± 0.03	1
B1430−178	2.331	19.4	18.82 ± 0.07	18.67 ± 0.06	15.68 ± 0.23	2
B1535+004	3.497	...	...	...	...	...
B1556−245	2.813	...	18.46 ± 0.06	18.69 ± 0.06	16.53 ± 0.31	2
B1635−035	2.871	...	20.06 ± 0.32	19.83 ± 0.20	17.36 ± 0.32	2
B1701+016	2.842	...	...	...	...	...
B1705+018	2.575	...	18.30 ± 0.07	18.07 ± 0.06	15.85 ± 0.10	2
B1937−101	3.780	...	...	...	...	...
B2000−330	3.780	...	18.34 ± 0.06	17.05 ± 0.05	15.05 ± 0.08	2
B2126−158	3.275	17.1	17.63 ± 0.05	16.66 ± 0.05	14.27 ± 0.05	2
B2149−307	2.330	18.4	17.89 ± 0.05	17.67 ± 0.05	15.21 ± 0.13	2
B2212−299	2.703	17.4	17.41 ± 0.05	17.31 ± 0.05	14.58 ± 0.06	2
B2215+020	3.550	22.0	21.61 ± 0.31	20.24 ± 0.10	19.30 ± 1.78	2
B2224+006	2.248	22.0	...	...	...	...
B2245−059	3.295	19.7	...	...	...	...
B2245−328	2.268	18.3	19.00 ± 0.07	18.76 ± 0.07	16.08 ± 0.19	2
B2256+017	2.663	19.6	...	...	...	...
B2311−373	2.476	18.4	18.99 ± 0.04	...	16.38 ± 0.04	1
B2314−340	3.100	18.3	...	...	...	...
B2314−409	2.448	19.0	18.26 ± 0.06	18.03 ± 0.05	15.58 ± 0.08	2
B2315−172	2.462	21.0	...	...	...	...
B2325−150	2.465	20.0	...	...	...	...
B2351−154	2.665	18.7	18.82 ± 0.07	18.60 ± 0.06	16.37 ± 0.26	2

Note.—Table 2 is also available in machine-readable form in the electronic edition of the *Astronomical Journal*.
References.—(1) This work; (2) FWW00.

images to the mode of the sequence. Bright objects were identified in the co-added frame and masked out before running through the co-addition process a second time.

The photometric solution was determined in a manner similar to the optical observations using IR photometric standards from Persson et al. (1998). Although the 2004 March run was photometric, cirrus was present at the end of the 2003 October run. For the affected SofI data, we determined K_s magnitudes by bootstrapping the photometric solution from Two Micron All Sky Survey (2MASS) point sources. Typically, five 2MASS point sources were available per field for the bootstrap calibration; the larger errors for the magnitudes of these QSOs reflect the rms in the fit to 2MASS magnitudes.[4] A filter transformation[5] was applied in order to place the SofI magnitudes on the Persson K_s system. However, in the absence of contemporaneous J-band magnitudes we have estimated the $J - K$ color as a function of $B - K$ using the data set of FWW00. Given the scatter in this color-color relation, we expect that the error in assuming a $J - K$ color will affect the filter transformation at <0.02 mag. The final quoted K_s-band errors in Table 2 include the uncertainty in the fit of the photometric solution, photon statistics, and the estimated error in the filter transformation added in quadrature.

Finally, both optical and IR colors were corrected for Galactic extinction according to the maps of Schlegel et al. (1998). Our final optical and IR magnitudes are presented in Table 2.

2.3. *Literature Magnitudes*

We have supplemented our measurements in Table 2 with magnitudes determined by FWW00, who also achieved near-simultaneous optical and IR (less than six nights' separation) observations of a number of CORALS QSOs. In Table 2 we have corrected the K_n-band magnitudes (deduced from the South African Astronomical Observatory system) given in FWW00 to K_s magnitudes by using the conversion determined by 2MASS.[6] We also corrected the photometry of FWW00 for Galactic extinction according to the maps of Schlegel et al. (1998).

With these supplemental data, we have optical–IR colors for 45 out of 66 program QSOs, with $B - K$ colors for 42. Of these 42, 14 have intervening DLA systems; only three QSOs with four intervening DLA systems were not observed by us or FWW00.[7] The observed subsample of CORALS QSOs is representative of the whole sample; only scheduling restrictions prevented the observation of the full sample. In the remainder of this paper we refer to the colors determined from our B and K_s magnitudes as $B - K$.

3. RESULTS

3.1. *Comparison of Optical and IR Colors*

The observed $B - K$ color of a given QSO will change with redshift as the intrinsic spectrum slides through the filter set. Strong emission features such as Lyα and C IV can increase the observed flux in a given band, although flux depression due to the Lyα forest is the dominant source of color shift (e.g., Richards et al. 2003). In Figure 5 we demonstrate this effect by calculating the change in $B - K$ as a function of redshift using the SDSS composite spectrum of Vanden Berk (2001). The color is calculated relative to a reference redshift, in this case $z = 2.3$. We therefore determine a normalized $B - K$, $(B - K)_n$, which is calculated in the following way. First, we determine the median $B - K = 2.92$ for QSOs in the range $2.2 < z < 2.4$, since the color changes very little over this interval (see Fig. 5). Next, we determine a redshift-dependent color correction based on the SDSS composite spectrum, displayed graphically in Figure 5. In the case of QSOs with intervening DLA systems, we make a correction $[\Delta(B - K)_{\rm DLA}]$ for the suppression of flux in the B band due to the Lyα line. For each DLA system, we simulate a spectrum with a damped profile at the redshift $z_{\rm abs}$ and with N(H I) given in Table 3. The spectrum is multiplied by the filter transmission curve and the resulting magnitude compared with an identical spectrum without a DLA absorber. Typical corrections are a few hundredths to a tenth of a magnitude, with a maximum $\Delta(B - K)_{\rm DLA} = 0.18$. The final, normalized $B - K$ color of each QSO is calculated by subtracting the median, the redshift-dependent term, and (in the case of an intervening DLA system) the absorption-correction term $[(B - K)_n = (B - K) - 2.92 - f(z) - \Delta(B - K)_{\rm DLA}]$.

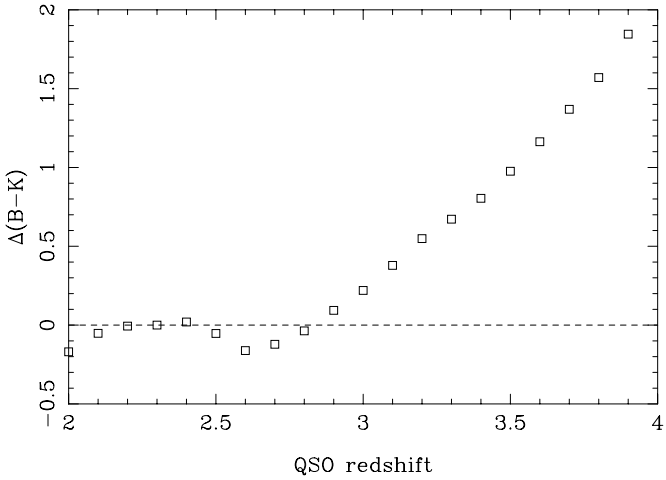

FIG. 5.—Change in $B - K$ color as a function of redshift determined using the SDSS composite spectrum of Vanden Berk (2001). Color changes are relative to $z = 2.3$.

Table 3 presents the normalized $B - K$ colors for the procedure described above, and Figure 6[8] demonstrates that the resulting color distribution does not exhibit any redshift dependence. There is, however, a large spread in $(B - K)_n$ at any given redshift, regardless of whether a DLA system is present, as expected for RLQs (e.g., FWW00).

3.2. *Limits on Extinction*

In order to determine quantitatively whether the colors of QSOs with and without DLA systems are drawn from the same distribution, we execute a Kolmogorov-Smirnov (K-S) test on two subsamples: the 14 QSOs with DLA systems and 25 without. The K-S test yields a 94% probability that the two subsamples are drawn from the same distribution. The mean (median) normalized colors of QSOs with DLA systems are +0.12 (+0.01) and of QSOs without DLA systems −0.10 (+0.02), with rms scatters

[4] One QSO, B0537−286, was observed during both 2003 October and 2004 March. The magnitude determined from the bootstrap analysis, $K = 16.11 \pm 0.04$, agrees (within the errors) with the magnitude determined under photometric conditions.

[5] See http://www.ls.eso.org/lasilla/sciops/ntt/sofi/setup/Zero_Point.html.

[6] See http://www.astro.caltech.edu/~jmc/2mass/v3/transformations.

[7] Ellison et al. (2001) reported 19 intervening DLA systems. However, one of these, the $z_{\rm abs} = 1.875$ DLA system toward B2314−409, has been shown by Ellison & Lopez (2001) to have an N(H I) slightly below the canonical DLA limit of 2×10^{20} cm^{-2}.

[8] In this figure, Table 3, and the following statistics, we only include QSOs whose B- and K_s-band magnitudes have errors less than 0.3 mag. In practice, this excludes only three of the FWW00 QSOs, which have poorer photometry. Our conclusions are unaffected by the exclusion of these three.

TABLE 3
NORMALIZED COLORS AND INTERVENING ABSORBER PROPERTIES FOR CORALS QSOs WITH NEAR-SIMULTANEOUS $B-K$ COLORS

QSO	z_{em}	z_{abs}	N(H I)	$(B-K)_n$	[Zn/H]	[Fe/H]	Abundance References
B0113−283	2.555	...	...	−0.49 ± 0.16	...	...	...
B0244−128	2.201	...	...	0.17 ± 0.11	...	...	...
B0325−222	2.220	...	...	0.02 ± 0.06	...	...	...
B0329−255	2.685	...	...	−0.68 ± 0.16	...	...	...
B0405−331	2.570	2.570	20.60	0.28 ± 0.06	<−0.49	−1.74	1
B0420+022	2.277	...	...	−0.12 ± 0.06	...	...	...
B0422−389	2.346	...	...	−0.42 ± 0.14	...	...	...
B0432−440	2.649	2.297	20.78	−0.41 ± 0.06	<−1.21	−1.45	1
B0434−188	2.702	...	...	0.21 ± 0.08	...	...	...
B0438−436	2.863	2.347	20.78	1.54 ± 0.05	−0.68	−1.30	1
B0451−282	2.560	...	...	0.07 ± 0.05	...	...	...
B0458−020	2.286	2.039	21.65	1.02 ± 0.05	−1.15	−1.61	1
B0528−250	2.765	2.141	20.75	−0.28 ± 0.05	−1.45	−1.57	1
		2.811	21.20	...	−0.47	−1.11	1
B0537−286	3.110	2.974	20.30	0.35 ± 0.08	<−0.40	...	1
B0919−260	2.300	...	...	0.09 ± 0.08	...	...	...
B0933−333	2.906	2.682	20.48	−0.06 ± 0.08	<−1.12	−1.54	1
B1010−427	2.954	...	...	−1.14 ± 0.08	...	...	...
B1055−301	2.523	1.904	21.54	0.16 ± 0.08	−1.26	−1.57	1
B1136−156	2.625	...	...	0.28 ± 0.08	...	...	...
B1147−192	2.489	...	...	0.42 ± 0.08	...	...	...
B1149−084	2.370	...	...	0.25 ± 0.08	...	...	...
B1228−113	3.528	2.193	20.60	0.19 ± 0.08	−0.22	...	1
B1228−310	2.276	...	...	−0.35 ± 0.08	...	...	...
B1230−101	2.394	1.931	20.48	−0.20 ± 0.08	−0.17	−0.63	1
B1256−243	2.263	...	...	0.17 ± 0.08	...	...	...
B1318−263	2.027	...	...	1.02 ± 0.08	...	...	...
B1354−107	3.006	2.501	20.40	0.08 ± .08	<−1.32	−1.25	1
		2.966	20.78	...	<−1.48	−1.54	1
B1402−012	2.518	...	...	0.02 ± 0.08	...	...	...
B1418−064	3.689	3.449	20.40	−0.43 ± 0.08	<−1.04	−1.72	1
B1430−178	2.331	...	...	0.21 ± 0.24	...	...	...
B1705+018	2.575	...	...	−0.34 ± 0.12	...	...	...
B2000−330	3.780	...	...	−1.16 ± 0.10	...	...	...
B2126−158	3.275	...	...	−0.20 ± 0.07	...	...	...
B2149−307	2.330	...	...	−0.25 ± 0.14	...	...	...
B2212−299	2.703	...	...	0.03 ± 0.08	...	...	...
B2245−328	2.268	...	...	0.00 ± 0.20	...	...	...
B2311−373	2.476	2.182	20.48	−0.32 ± 0.06	<−1.29	−1.70	1
B2314−409	2.448	1.857	20.90	−0.23 ± 0.10	−1.02	−1.33	2
		1.875	20.10	...	<−1.19	−1.88	2
B2351−154	2.665	...	...	−0.34 ± 0.27	...	...	...

REFERENCES.—(1) Akerman et al. 2005; (2) Ellison & Lopez 2001.

of 0.56 and 0.47, respectively. A Student's t-test yields a test statistic = 1.32, indicating that the mean colors of the two samples are not significantly different.

In order to quantify a limit to the amount of reddening associated with the DLA systems in our sample, we run a series of simulations that artificially include/remove reddening in the spectra of QSOs with DLA systems. We then calculate the K-S statistic compared with the no-DLA sample. In each simulation, we redden the observed $B-K$ color of those QSOs with DLA systems assuming a fixed $E(B-V)$ for each DLA system for both Galactic and SMC extinction curves. We use the parameterizations of SMC ($R_V = 2.93$) and Galactic ($R_V = 3.08$) extinction from Pei (1992) and a second functional fit to Galactic reddening from CCM89, as described in § 1.3. The colors of QSOs without DLA systems remain unchanged in these simulations.

To demonstrate how a small change in $E(B-V)$ can affect the color distribution and K-S statistic, we show the $B-K$ colors for a range of simulations in Figures 7 and 8. The corresponding K-S probability is given in each panel. The results of the full simulation gamut for the three extinction curves are shown in Figure 9, where a positive $E(B-V)$ indicates that the spectrum was reddened, whereas a negative value indicates that the effects of dust were removed. These simulations rule out $E(B-V) > 0.04$ (SMC) and $E(B-V) > 0.07$ (MW) at 99% confidence [i.e., KS probability ≤ 0.01 for $E(B-V) < -0.04$, -0.07, with no difference between the Pei and CCM89 Galactic models].

Alternatively, we can consider a reddening that depends on the N(H I) of each DLA system. Reddening-to-gas[9] ratios have been determined in local galaxies, e.g.,

$$E(B-V) = \frac{N(\mathrm{H\ I})}{4.0 \times 10^{22}} \quad (1)$$

[9] Some authors refer to the relationship between $E(B-V)$ and N(H I) as a dust-to-gas ratio. However, we prefer to use the term "reddening-to-gas ratio" to avoid confusion with the parameters k and κ that are often used in the literature to denote dust-to-gas ratios inferred, for example, from chemical abundances.

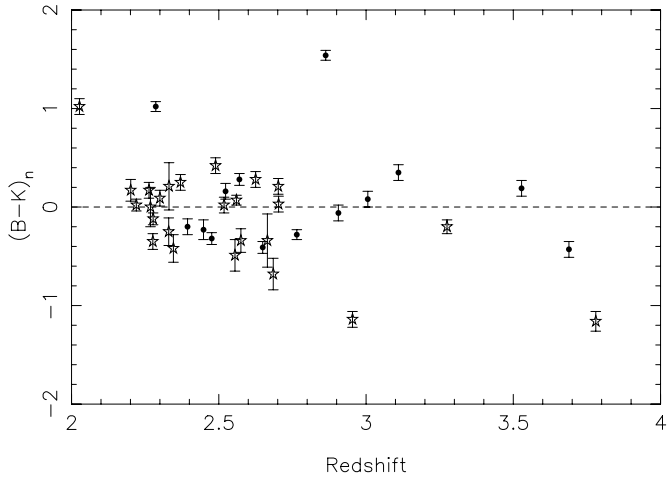

FIG. 6.—Redshift distribution of normalized $B-K$ colors for QSOs with (*circles*) and without (*stars*) DLA systems. [*See the electronic edition of the Journal for a color version of this figure.*]

for the SMC (Bouchet et al. 1985) and

$$E(B-V) = \frac{N(\mathrm{H\ I})}{5.8 \times 10^{21}} \quad (2)$$

for the MW (Bohlin et al. 1978).

If reddening is removed from the DLA-QSO sample in accordance with the SMC reddening-to-gas relation in equation (1), the K-S probability is 0.39, an inconclusive result. Correcting the colors of QSOs with DLA systems using the more extreme Galactic relation in equation (2) results in colors that are significantly bluer than the no-DLA QSOs; i.e., the reddening correction is too large. The K-S probability in this case is 0.03, ruling out a Galactic reddening-to-gas relation at 2 σ.

In reality, reddening is likely to be more stochastic than the simple dust recipes adopted here, and extinction curves are likely to vary from DLA system to DLA system. Our data set is currently too small to quantify the reddening-to-gas ratios for DLA systems through modeling techniques such as χ^2 minimization, although we can rule out a Galactic scaling relation at 97% confidence. However, future work with larger samples, e.g., with DLA systems identified from the SDSS, will be able to investigate the reddening-to-gas relation in more detail. Finally, we note that a detailed treatment of other effects, such as nonnegligible intergalactic medium reddening, host galaxy contributions, or exotic extinction laws, are beyond the scope of this paper.

3.3. *X-Ray Observations of the Reddest QSOs*

To further investigate the three QSOs with the reddest $B-K$ colors, we have searched for archival X-ray observations of these sources. Given a sufficient signal-to-noise ratio in the X-ray data, it is possible to investigate whether intrinsic absorption (i.e., associated with the QSO) is present. In principle, the X-ray data can measure, or place constraints on, the integrated hydrogen column along the line of sight (and, by assuming a dust-to-gas ratio, on the reddening), as well as the redshift at which the absorption takes place. Since the inferred N(H I) column densities of intrinsic absorbers are frequently an order of magnitude higher than typical intervening DLA systems, it is plausible

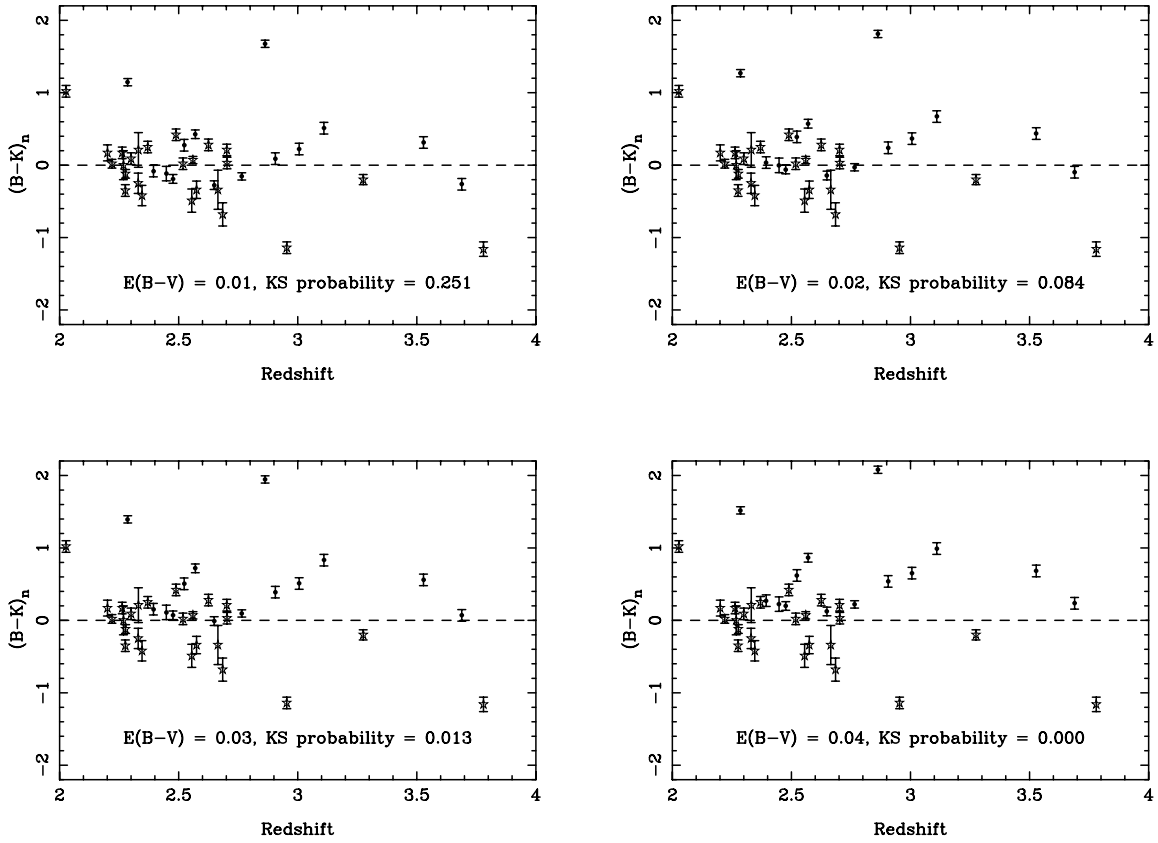

FIG. 7.—Redshift distribution of normalized $B-K$ colors for QSOs with (*circles*) and without (*stars*) DLA systems with reddening *added* to the former population assuming a Pei (1992) SMC extinction law. Each of the four panels illustrates a different degree of reddening and shows the K-S probability that the DLA and no-DLA QSOs are drawn from the same color distribution. [*See the electronic edition of the Journal for a color version of this figure.*]

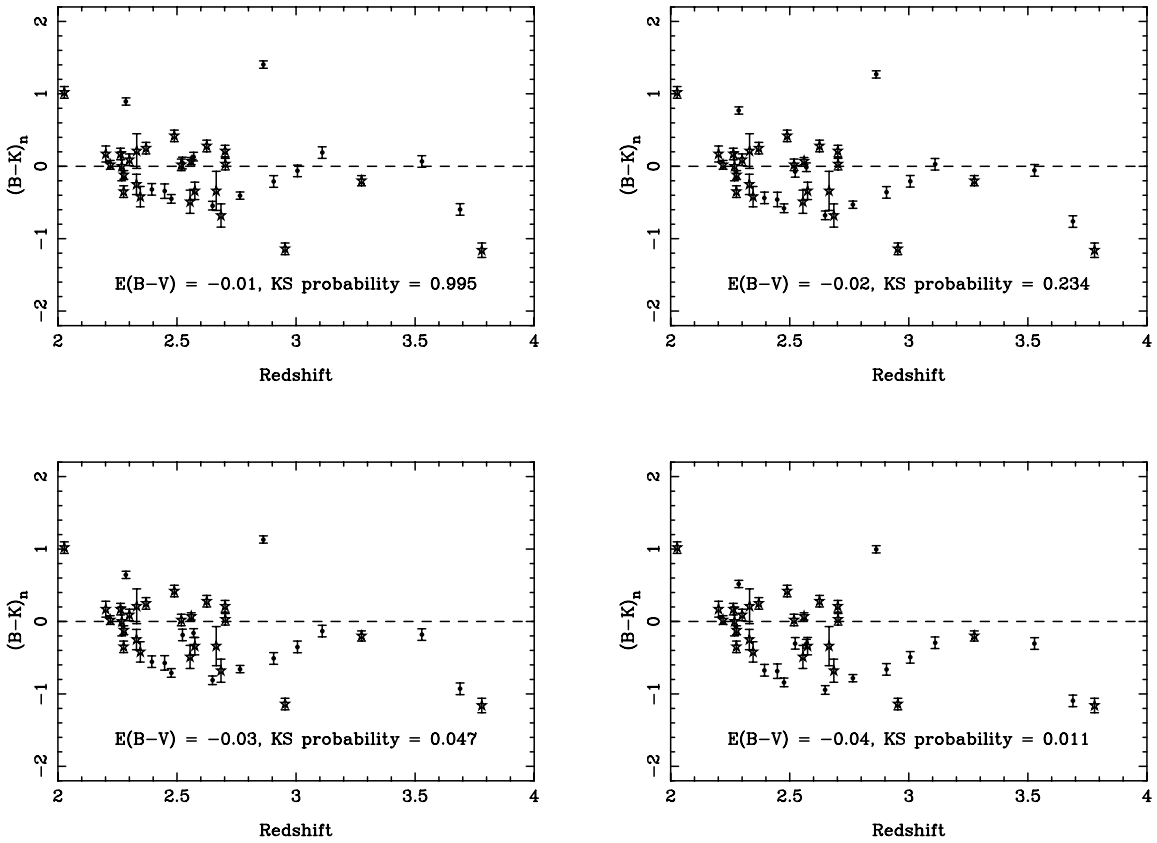

FIG. 8.—Same as Fig. 7, but with reddening *removed* from the former population. [*See the electronic edition of the Journal for a color version of this figure.*]

that significant reddening may be induced by such an absorber (although an important caveat is the large possible range in the reddening-to-dust ratios).

Of the three sources with $(B-K)_n > 1$ we found that X-ray observations had been obtained for the QSOs B0438−436 and B0458−020, both of which exhibit DLA absorption. Unfortunately, no X-ray observations have been obtained for B1318−263, the system without a DLA absorber.

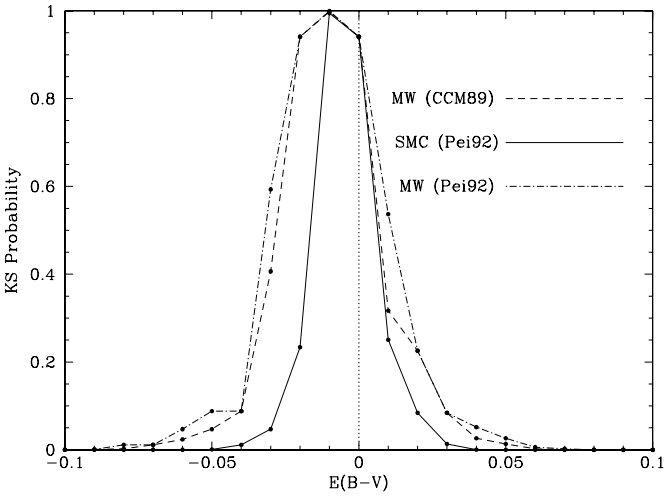

FIG. 9.—K-S probability that the $(B-K)_n$ colors of QSOs with and without DLA systems are drawn from the same distribution, for simulations that include reddening in the former population. Positive values of $E(B-V)$ indicate that the effect of dust (i.e., reddening) was added to the simulated spectra, and negative values indicate that the effect of dust was removed. The vertical dotted line indicates that the raw $(B-K)_n$ colors have been used, i.e., no reddening is included. [*See the electronic edition of the Journal for a color version of this figure.*]

B0438−436 has long been known to exhibit significant excess (i.e., above the Galactic contribution) absorption. Evidence for this excess absorption has come from the analysis of *ROSAT*, *ASCA*, and *XMM-Newton* observations (Serlemitsos et al. 1994; Elvis et al. 1994; Cappi et al. 1997; Brocksopp et al. 2004). The best-quality data so far are those obtained with *XMM-Newton*, and the best-fit model (Brocksopp et al. 2004) is consistent with a solar metallicity absorber with $N(\mathrm{H}) = 1.3 \times 10^{22}$ cm^{-2}, which Brocksopp et al. assumed to be at the redshift of the QSO.[10] If we assume that ionized and molecular gas is negligible, this column density translates into $E(B-K) \sim 18.5$ and ~ 5 for a Galactic and SMC reddening-to-dust ratio, respectively, and extinction curves from Pei (1992). These values are considerably higher than the $E(B-K)$ observed for this source (see Fig. 6). While there are a number of explanations for this discrepancy (e.g., dustless gas near the QSO or active galactic nucleus extinction curves that are significantly different from Local Group galaxies, e.g., Gaskell et al. 2004), a large reddening due to associated absorption is very plausible.

We have retrieved archival *Chandra* ACIS data for B0458−020 (ObsID 2985) with a total exposure of 77.76 ks. The data were analyzed in the 0.3–10.0 keV energy range using CIAO 3.2.1 software and the latest calibration files. B0458−020 suffers from relatively high Galactic absorption, corresponding to $N(\mathrm{H\ I}) = 7.5 \times 10^{20}$ cm^{-2}, which hinders the detection of intrinsic absorption that is redshifted to the soft (low-energy) part of the spectrum. Indeed, a spectral fit assuming a simple power-law spectrum with only Galactic absorption yields a good fit to

[10] With sufficiently high quality data, it is possible to determine the absorption redshift. However, associated absorption is often the working assumption, since the column densities greatly exceed those of typical intervening absorbers. In this case, the intervening DLA systems have $N(\mathrm{H\ I}) = 6 \times 10^{20}$ cm^{-2}.

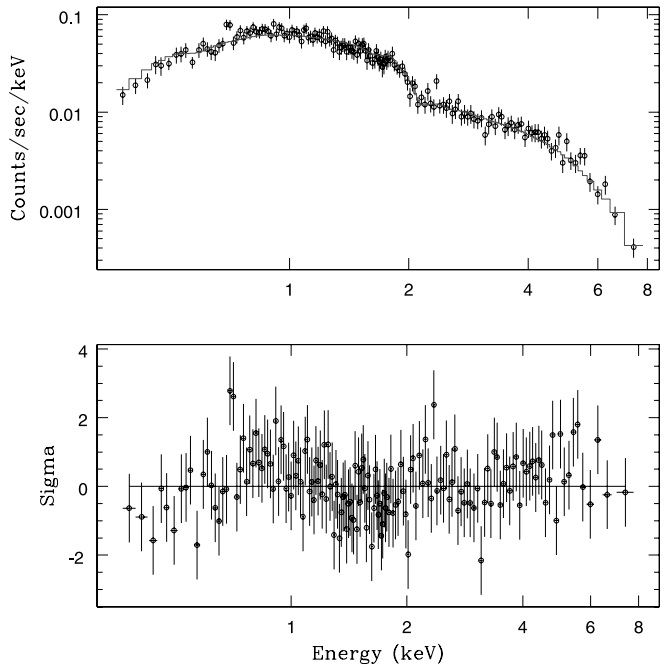

FIG. 10.—Best-fit χ^2 plots of the B0458−020 *Chandra* observations. The fit and σ [(data−model)/error] plots are shown after convolving with the instrument response (*top and bottom, respectively*). The data were fitted with a single power-law model absorbed by a Galactic foreground N(H I) column (*solid line, top*). [*See the electronic edition of the Journal for a color version of this figure*.]

the data, i.e., $\chi^2_{\rm red} = 0.8$ for 155 degrees of freedom. The best-fit photon index Γ ($f_\nu \propto \nu^{\Gamma+1}$ ergs s^{-1} cm^{-2}) was found to be 1.55 ± 0.02 (see Fig. 10). The inclusion of absorption at either the QSO or the DLA redshift gave no significant improvement to the fit: $N({\rm H}) < 2 \times 10^{21}$ cm^{-2} with 99% confidence (F-test statistics $F \sim 0.002$ for $\Delta\chi^2 \sim 7.3$ and one additional parameter). Using the Pei (1992) extinction laws, this corresponds to an upper limit $E(B-K) < 2.8$ and <0.7 for a Galactic and SMC, respectively, reddening-to-dust ratio if the absorber is located in the host galaxy. Associated absorption could therefore be the cause of the red color of this QSO, although better X-ray data would be required to confirm this. However, we note that Carilli et al. (1998) found that 80% of red QSOs in their sample exhibited strong 21 cm absorption at the QSO redshift, supporting the view that red colors may often be caused by intrinsic absorption.

4. DISCUSSION

In a series of papers, Fall & Pei (1989), Fall et al. (1989), and Pei et al. (1991) investigated whether the spectral indices of QSOs with DLA systems were systematically steeper than QSOs with no intervening galaxy. In particular, in the latter of these papers, new data with higher spectrophotometric accuracy were obtained and a sample of 66 QSOs analyzed for reddening. The distribution of spectral indices in the DLA sample (20 QSOs) was found to differ at the 99.999% confidence level from the no-DLA (46 QSOs) sample. The inferred dust-to-gas ratio was 5%–20% of that in the MW. Further support for observed reddening was reported by Outram et al. (2001), who found redder $B-R$ colors for QSOs with $0.5 < z < 1.5$ high equivalent width Mg II absorbers. The inferred color excess was $E(B-V) \sim 0.04$. More recently, Wild & Hewett (2005) found a convincing reddening signature associated with low-z Ca II absorbers in the SDSS, although still at a modest level: $E(B-V) = 0.06$. Individual cases of DLA reddening have been reported based on either differential reddening in lensed systems (e.g., Zuo et al. [1997] for a DLA system at $z_{\rm abs} = 1.4$) or the detection of the 2175 Å graphite feature (Junkkarinen et al. [2004] for a DLA system at $z_{\rm abs} = 0.5$). However, some caution is required when comparing inferences on dust extinction at different redshift ranges, since the amount, source, and composition of dust may differ, for example, as the dominant source of dust shifts from Type II supernovae to lower mass stars (e.g., Hirashita et al. 2005). Nonetheless, these works apparently provide robust evidence for the systematic reddening of QSOs with intervening absorption systems at both high and low redshifts.

Recently, however, Murphy & Liske (2004) revisited the spectral-fitting approach with a large statistical sample drawn from the SDSS. In addition to its size (∼1450 QSOs, with 72 DLA systems), this sample has the advantage that its data acquisition is homogeneous and the spectral indices are fit over a wider wavelength range than was done in earlier work. With these improvements, Murphy & Liske (2004) find no steepening of the spectral indices for QSOs with DLA systems and determine a limit of $E(B-V) < 0.02$ (99% confidence). Although Murphy & Liske adopt a similar approach to that of Fall, Pei, and collaborators in fitting spectral indices, they do so with an order of magnitude larger sample, wider wavelength coverage, and uniform data acquisition. Since QSOs have a wide range of intrinsic colors and spectral shapes, using the broadest baseline possible is important for identifying a systematic dust reddening.

For the first time, optical–IR colors can now contribute to the ongoing debate. Although our sample is modest in size in comparison with the SDSS (although comparable with the samples of Pei, Fall, and collaborators), the broad wavelength coverage provides significant leverage for detecting reddening. For example, whereas the $B-K$ color changes by 0.74 for an $E(B-V) = 0.05$ (SMC extinction $z_{\rm em} = 3.0$, $z_{\rm abs} = 2.6$), the $B-R$ color changes by only 0.35. Moreover, the sample of QSOs on which we conduct this work is based on an optically complete survey of radio-loud quasars. Therefore, our sample of DLA systems should not be subject to selection effects associated with dust extinction.

Our results are presented graphically in Figure 6, where we show the normalized $B-K$ colors for QSOs with and without DLA systems. The mean color of QSOs without DLA systems is -0.10, compared with +0.12 for the DLA subsample. Both color distributions have rms scatters of ∼0.5. Neither a Student's t-test nor a K-S test find any significant difference in the $B-K$ colors of the two subsamples. We determine a 3 σ limit of $E(B-V) <$ 0.04 and 0.07 for SMC and Galactic extinction, respectively, based on the results of our K-S test simulations. Although not quite as sensitive as limits from the SDSS (Murphy & Liske 2004), our sample is optically complete and could potentially contain heavily extinguished QSOs that would not have been found in magnitude-limited samples. However, the low $E(B-V)$ allowed by this work shows that even in optically complete samples, the amount of reddening is small. Such low values of $E(B-V)$ are consistent with the small H_2 fractions observed in DLA systems; while a handful of absorbers have $\log f({\rm H_2}) \sim -2$, most have $\log f({\rm H_2}) < -5$ (Ledoux et al. 2003). Indeed, Tumlinson et al. (2002) have shown that low molecular fractions are common in Galactic and Magellanic Cloud sight lines when $E(B-V) \lesssim 0.08$.

Although this work has not found any indication that QSOs are significantly reddened by intervening DLA systems, evidence that *some* dust is present in DLA systems is well established from the abundances of refractory versus volatile elements such as Cr and Zn (e.g., Pettini et al. 1994, 1997). Akerman et al. (2005) have obtained Zn and Fe abundances for many of the

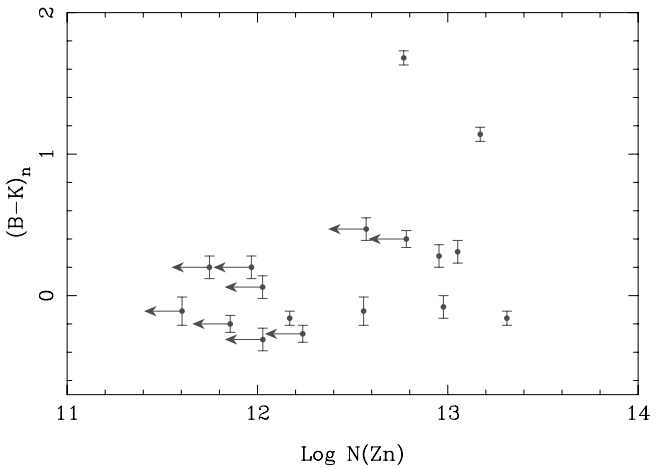

FIG. 11.—Normalized $B-K$ color of CORALS DLA systems as a function of Zn column density. [*See the electronic edition of the Journal for a color version of this figure*.]

DLA systems in our sample; we reproduce these abundance results in Table 3, adopting the solar reference values from Lodders (2003). Vladilo & Péroux (2005) have recently suggested that reddening will increase linearly with N(Zn) and become especially severe when $\log N(\mathrm{Zn}) > 13.2$. In Figure 11 we plot the normalized $B-K$ color versus N(Zn) using the column densities reported in Akerman et al. (2005).[11] We detect no trend between normalized color and $\log N$(Zn), although we have only three DLA systems with $\log N(\mathrm{Zn}) > 13.0$. Nonetheless, Akerman et al. (2005) find that the mean weighted metallicity of CORALS DLA systems is only marginally higher (although consistent within the error bars) than previous samples.

In Figure 12 we investigate whether there is any correlation between N(H I) or depletion (as measured by [Fe/Zn]) and reddening. The two reddest QSOs that also show DLA absorption have slightly larger than average ($[\mathrm{Fe/Zn}] = -0.3$; Prochaska & Wolfe 2002) but still modest depletions. The rest of the sample (including two systems with comparable depletions to the reddest DLA-harboring QSOs) do not show any correlation between depletion and reddening. Similarly, the N(H I) of one of the three very red QSOs in our sample has the DLA system with the highest N(H I) among CORALS absorbers. However, a second high-N(H I) DLA system has apparently not reddened its background QSO to a similar extent, and the reddest QSO with a DLA system has only a modest N(H I). Overall, there is no obvious trend between $(B-K)_n$ and N(H I). On the other hand, Khare et al. (2004) do report tentative evidence for a correlation between the inferred $E(B-V)$ (based on broadband SDSS colors) and [Cr/Zn] (analogous to the [Fe/Zn] plotted in Fig. 12). However, the Khare et al. result is based on the two systems in their sample with $[\mathrm{Cr/Zn}] < 1$, and only one of the DLA systems in our sample may have such a high dust-to-gas ratio. The normalized $B-K$ color of this QSO is mildly redder than the median color of the other QSOs, although this certainly cannot be taken as evidence for a correlation between depletion and reddening. It would be of great interest to further investigate the correlation between reddening and dust-to-gas ratio in a larger sample of objects.

[11] We make the usual assumption that Zn II is the dominant ionization stage of this element and that the contribution from other ionization stages is negligible. Moreover, in Figs. 11 and 12 we include two DLA systems within 3000 km s^{-1} of the QSO, plus one further absorber whose N(H I) is just below the canonical DLA limit.

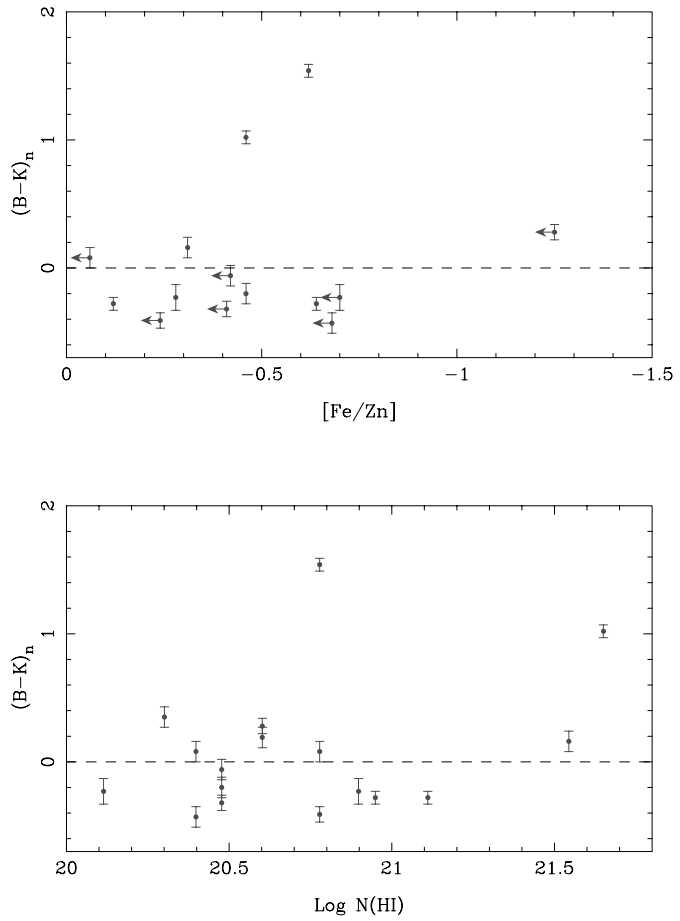

FIG. 12.—*Top*: Normalized $B-K$ color as a function of depletion, as measured by [Fe/Zn]. *Bottom*: Normalized $B-K$ color as a function of neutral hydrogen column density, N(H I). [*See the electronic edition of the Journal for a color version of this figure*.]

Prantzos & Boissier (2000) have suggested that dust bias is responsible for the observed anticorrelation between [Zn/H] and N(H I) and propose an empirical "dust filter," i.e., that DLA systems in optically selected samples all have $\log N(\mathrm{H\ I}) + [\mathrm{Zn/H}] < 21$. In Figure 13 we plot N(H I) versus [Zn/H] from the compilation of DLA systems in Kulkarni et al. (2005); the dust filter suggested by Prantzos & Boissier (2000) is shown by the dashed line. We can combine the suggested cutoff of $\log N(\mathrm{H\ I}) + [\mathrm{Zn/H}] < 21$ with a reddening-to-gas ratio that scales with metallicity in order to calculate what $E(B-V)$ is implied. For example, it is straightforward to show that if the Galactic reddening-to-gas ratio given in equation (2) is scaled by [Zn/H] and satisfies the criterion $\log N(\mathrm{H\ I}) + [\mathrm{Zn/H}] < 21$, then $E(B-V) < 0.17$. This is the $E(B-V)$ value required to ensure that no high-N(H I), high-[Zn/H] systems are observed; $E(B-V) = 0.17$ is indeed considerably larger than the limits determined by this work and that of Murphy & Liske (2004). We can alternatively calculate where the observed cutoff in Figure 13 would lie for a given assumed $E(B-V)$. For example, an $E(B-V) < 0.05$ implies $\log N(\mathrm{H\ I}) + [\mathrm{Zn/H}] < 20.46$ (again using eq. [2] scaled by $10^{[\mathrm{Zn/H}]}$); this cutoff is shown in Figure 13 by a dot-dashed line. If future work determines an $E(B-V) \ll 0.05$, it may (depending on the assumed reddening-to-gas ratio) become difficult to quantitatively reconcile the N(H I)-[Zn/H] distribution with dust bias.

In Figure 13 we also plot the N(H I) and [Zn/H] values for the CORALS DLA systems, which should not be subject to dust bias. The figure shows that CORALS DLA systems are not

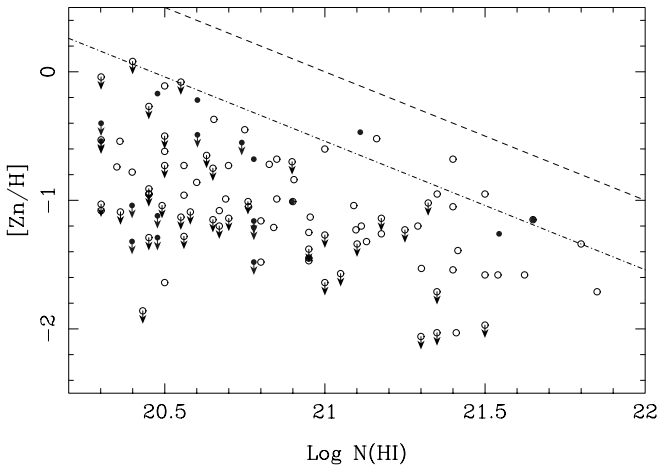

FIG. 13.—Metallicity vs. N(H I) column density for DLA systems taken from the compilation of Kulkarni et al. (2005) and for the CORALS DLA systems (Akerman et al. 2005) (*open and filled circles, respectively*). The dashed line shows the proposed dust filter of Prantzos & Boissier (2000), $\log N(\mathrm{H\ I}) + [\mathrm{Zn/H}] < 21$, which corresponds to $E(B-V) < 0.17$ for a Galactic gas-to-reddening law scaled by metallicity. The dot-dashed line shows where the cutoff would lie if $E(B-V) < 0.05$, i.e., $\log N(\mathrm{H\ I}) + [\mathrm{Zn/H}] < 20.46$. [*See the electronic edition of the Journal for a color version of this figure*.]

distinguishable from other (literature) DLA systems in terms of their N(H I)-[Zn/H] distribution. Moreover, they do not lie above the empirical cutoff, which has been proposed to be due to dust. However, in the chemical evolution models of Churches et al. (2004), $\lesssim$9% of DLA systems (depending on the choice of spin parameter) are expected to be in this "dust-forbidden" region (A. Nelson 2005, private communication). It therefore seems premature at this point to interpret the lack of high-N(H I), metal-rich CORALS DLA systems as evidence that the anticorrelation is not caused by dust.

If future work concludes that dust *is* the reason for the anticorrelation in Figure 13, then the locus of data points compared with the theoretical lines and the lack of high CORALS values may indicate that typical $E(B-V)$ values are simply intrinsically low in most DLA systems. Indeed, Ellison et al. (2005) found $E(B-V) \lesssim 0.2$ even in the central parts of absorber counterparts at $z < 0.5$. Alternatively, the implied $E(B-V)$ values from this and the work of Murphy & Liske (2004) may be explained if the dust extinction is relatively gray, as has been proposed to explain the $E(B-V)$ values observed toward some gamma-ray burst hosts (e.g., Vreeswijk et al. 2004).

One of the greatest uncertainties in this work is the unknown nature (i.e., composition, grain size, and, therefore, extinction curve) of dust in damped systems. The main observational distinction between SMC and Galactic extinction curves (with the LMC being somewhat intermediate between the two; see Fig. 1) is the presence of a "bump" at 2175 Å attributed to graphite. A handful of detections of this feature at cosmological redshifts exist, associated with three Mg II absorbers with $z_{\mathrm{abs}} \sim 1.5$ in the SDSS (Wang et al. 2004), a high-N(H I) DLA system at $z_{\mathrm{abs}} \sim 0.5$ (Junkkarinen et al. 2004), and several cases of galaxy lenses (e.g., Falco et al. 1999; Toft et al. 2000; Motta et al. 2002; Wucknitz et al. 2003; Munoz et al. 2004). However, gravitationally lensed systems are clearly special cases, since the impact parameter through the galaxy is necessarily small. Malhotra (1997) has claimed to see the 2175 Å feature in stacked (unlensed) QSO spectra exhibiting Mg II absorption, although stacks of SDSS spectra have failed to reproduce this (M. Murphy 2005, private communication; Ménard 2005; Khare et al. 2005; Wild & Hewett 2005). Although further investigation is warranted, this may be evidence that Galactic dust is not generally applicable for absorbers toward unlensed QSOs. Theoretical models of dust in high-redshift galaxies enriched by high-mass Type II supernovae may be more relevant than local extinction curves. However, the extinction properties among these models also vary tremendously depending on progenitor mass and mixing (e.g., Hirashita et al. 2005).

5. CONCLUSIONS

In this work we have investigated whether dust in DLA systems can cause a significant, systematic reddening of background QSOs by obtaining $B-K$ colors for an optically complete, radio-selected quasar sample. We determine normalized colors that account for redshift dependence (analogous to a K-correction, which accounts for Lyα flux decrement and emission lines) and suppressed B-band flux due to DLA absorption. The mean normalized $B-K$ color of the DLA subsample is 0.12 ± 0.56, compared with -0.10 ± 0.47 for the no-DLA subsample. Both a Student's t-test and a K-S test indicate that there is no statistical difference between the distribution of $B-K$ colors in the two subsamples. We place a limit on the amount of reddening that may be present by correcting the colors of QSOs with DLA systems using a range of $E(B-V)$ values. Adopting an SMC extinction curve, we place a 3 σ limit on the systematic reddening: $E(B-V) < 0.04$, assuming a fixed reddening for each DLA system. In general, there is no correlation between depletion, N(Zn), or N(H I) and reddening. Finally, we have searched for archival X-ray data of the three reddest QSOs in our sample in order to test whether their extreme $(B-K)_n$ colors may be due to intrinsic (i.e., at $z \sim z_{\mathrm{em}}$) absorption. Of these three QSOs, two have data available, and the spectrum of one (B0438−436) shows evidence for a high-N(H I) absorber associated with the QSO that may be the cause of the very red color.

These results support relatively low extinctions toward high-redshift DLA systems and agree with the $E(B-V)$ values inferred from the optically selected SDSS work of Murphy & Liske (2004). Therefore, although a handful of individual absorbers may cause more severe reddening (e.g., Junkkarinen et al. 2004), these seem to be the exception rather than the rule. A number of observational works have also inferred relatively small reddening at lower redshifts (e.g., Khare et al. 2005; Ménard 2005; Wild & Hewett 2005). Combined with previous work, which has found that the number density and gas content of intervening absorbers (Ellison et al. 2001, 2004) and their metallicities (Akerman et al. 2005) are not largely different from samples whose optical completeness exceeds $B \sim 19$, it seems increasingly unlikely that dust bias has severely skewed our view of high-redshift DLA systems. Put another way, the red (reddened) QSO population is unlikely to be linked to dust in high-redshift DLA systems.

The authors would like to thank the ever-expert help of the La Silla Observatory staff, especially Valentin Ivanov. S. L. E. is grateful to Jon Willis for providing advice regarding the reduction of the SofI data presented here. We are also grateful to Paul Francis for making the data presented in FWW00 available in electronic format and for additional information on that data set. S. L. E. also acknowledges informative discussions with Michael Murphy and is grateful for his feedback on an earlier draft of this work. P. L. acknowledges financial support by Fondecyt's grant 1040719. This publication makes use of data

products from the Two Micron All Sky Survey, which is a joint project of the University of Massachusetts and the Infrared Processing and Analysis Center, California Institute of Technology, funded by the National Aeronautics and Space Administration and the National Science Foundation. This work also makes use of the NASA Extragalactic Database.

REFERENCES

Akerman, C. J., Ellison, S. L., Pettini, M., & Steidel, C. C. 2005, A&A, in press (astro-ph/0506180)
Barkhouse, W., & Hall, P. B. 2001, AJ, 121, 2843
Benn, C. R., Vigotti, M., Carballo, R., Gonzalez-Serrano, J. I., & Sanchez, S. F. 1998, MNRAS, 295, 451
Bohlin, R. C., Savage, B. D., & Drake, J. F. 1978, ApJ, 224, 132
Bouchet, P., Lequeux, J., Maurice, E., Prevot, L., & Prevot-Burnichon, M. L. 1985, A&A, 149, 330
Bregman, J. N., Glassgold, A. E., Huggins, P. J., Lebofsky, M. J., Rieke, G. H., Aller, M. F., Aller, H. D., & Hodge, P. E. 1981, Nature, 293, 714
Brocksopp, C., Puchnarewicz, E. M., Mason, K. O., Cordova, F. A., & Priedhorsky, W. C. 2004, MNRAS, 349, 687
Cappi, M., Matsuoka, M., Comastri, A., Brinkmann, W., Elvis, M., Palumbo, G. G. C., & Vignali, C. 1997, ApJ, 478, 492
Cardelli, J. A., Clayton, G. C., & Mathis, J. S. 1989, ApJ, 345, 245 (CCM89)
Carilli, C. L., Menten, K. M., Reid, M. J., Rupen, M. P., & Yun, M. 1998, ApJ, 494, 175
Churches, D. K., Nelson, A. H., & Edmunds, M. G. 2004, MNRAS, 347, 1234
Draine, B. T. 2003, ARA&A, 41, 241
Drinkwater, M., Wiklind, T., & Combes, F. 1996, A&A, 312, 771
Ellison, S. L., Churchill, C. W., Rix, S. A., & Pettini, M. 2004, ApJ, 615, 118
Ellison, S. L., Kewley, L. J., & Mallén-Ornelas, G. 2005, MNRAS, 357, 354
Ellison, S. L., & Lopez, S. 2001, A&A, 380, 117
Ellison, S. L., Yan, L., Hook, I., Pettini, M., Wall, J., & Shaver, P. 2001, A&A, 379, 393
Elvis, M., Fiore, F., Wilkes, B., McDowell, J., & Bechtold, J. 1994, ApJ, 422, 60
Falco, E. E., et al. 1999, ApJ, 523, 617
Fall, S. M., & Pei, Y. 1993, ApJ, 402, 479
Fall, S. M., Pei, Y., & McMahon, R. G. 1989, ApJ, 341, L5
Francis, P., Whiting, M., & Webster, R. 2000, Publ. Astron. Soc. Australia, 17, 56 (FWW00)
Gaskell, C. M., Goosmann, R. W., Antonucci, R. R. J., & Whysong, D. H. 2004, ApJ, 616, 147
Glikman, E., Gregg, M. D., Lacy, M., Helfand, D. J., Becker, R. H., & White, R. L. 2004, ApJ, 607, 60
Gregg, M. D., Wisotzki, L., Becker, R. H., Maza, J., Schechter, P. L., White, R. L., Brotherton, M. S., & Winn, J. N. 2000, AJ, 119, 2535
Hirashita, H., Nozawa, T., Kozasa, T., Ishii, T. T., & Takeuchi, T. T. 2005, MNRAS, 357, 1077
Hopkins, P. F., et al. 2004, AJ, 128, 1112
Hutchings, J. B., & Giasson, J. 2001, PASP, 113, 1205
Junkkarinen, V. T., Cohen, R. D., Beaver, E. A., Burbidge, E. M., Lyons, R. W., & Madejski, G. 2004, ApJ, 614, 658
Khare, P., Kulkarni, V. P., Lauroesch, J. T., York, D. G., Crotts, A. P. S., & Nakamura, O. 2004, ApJ, 616, 86
Khare, P., et al. 2005, in IAU Colloq. 199, Probing Galaxies through Quasar Absorption Lines, ed. P. R. Williams, C. Shu, & B. Ménard (Cambridge: Cambridge Univ. Press), in press (astro-ph/0504532)
Kulkarni, V., Fall, S. M., Lauroesch, J. T., York, D. G., Welty, D. E., Khare, P., & Truran, J. W. 2005, ApJ, 618, 68
Landolt, A. 1992, AJ, 104, 340
Ledoux, C., Petitjean, P., & Srianand, R. 2003, MNRAS, 346, 209
Lodders, K. 2003, ApJ, 591, 1220
Malhotra, S. 1997, ApJ, 488, L101
Mathis, J. S. 1990, ARA&A, 28, 37
Ménard, B. 2005, in IAU Colloq. 199, Probing Galaxies through Quasar Absorption Lines, ed. P. R. Williams, C. Shu, & B. Ménard (Cambridge: Cambridge Univ. Press), in press
Meyer, D. M., & Roth, K. C. 1990, ApJ, 363, 57
Meyer, D. M., & York, D. G. 1992, ApJ, 399, L121
Motta, V., et al. 2002, ApJ, 574, 719
Muñoz, J. A., Falco, E. E., Kochanek, C. S., McLeod, B. A., & Mediavilla, E. 2004, ApJ, 605, 614
Murphy, M. T., & Liske, J. 2004, MNRAS, 354, L31
Nestor, D. B., Turnshek, D. A., & Rao, S. M. 2005, ApJ, 628, 637
Outram, P. J., Smith, R. J., Shanks, T., Boyle, B. J., Croom, S. M., Loaring, N. S., & Miller, L. 2001, MNRAS, 328, 805
Pei, Y. 1992, ApJ, 395, 130
Pei, Y., & Fall, S. M. 1995, ApJ, 454, 69
Pei, Y., Fall, S. M., & Bechtold, J. 1991, ApJ, 378, 6
Pei, Y., Fall, S. M., & Hauser, M. G. 1999, ApJ, 522, 604
Persson, S. E., Murphy, D. C., Krzeminski, W., Roth, M., & Rieke, M. J. 1998, AJ, 116, 2475
Pettini, M., Smith, L. J., Hunstead, R. W., & King, D. L. 1994, ApJ, 426, 79
Pettini, M., Smith, L. J., King, D. L., & Hunstead, R. W. 1997, ApJ, 486, 665
Prantzos, N., & Boissier, S. 2000, MNRAS, 315, 82
Prochaska, J. X., & Wolfe, A. M. 2002, ApJ, 566, 68
Rawlings, S., Lacy, M., Sivia, D. S., & Eales, S. A. 1995, MNRAS, 274, 428
Richards, G. T., et al. 2003, AJ, 126, 1131
Schlegel, D. J., Finkbeiner, D. P., & Davis, M. 1998, ApJ, 500, 525
Serlemitsos, P., Yaqoob, T., Ricker, G., Woo, J., Kunieda, H., & Terashima, Y. 1994, PASJ, 46, L43
Smith, H. E., & Spinrad, H. 1980, ApJ, 236, 419
Stein, W. A., & Sitko, M. L. 1984, AJ, 89, 1688
Stern, D., Hall, P. B., Barrientos, L. F., Bunker, A. J., Elston, R., Ledlow, M. J., Raines, S. N., & Willis, J. 2003, ApJ, 596, L39
Toft, S., Hjorth, J., & Burud, I. 2000, A&A, 357, 115
Tumlinson, J., et al. 2002, ApJ, 566, 857
Vanden Berk, D. E., et al. 2001, AJ, 122, 549
Vladilo, G., & Péroux, C. 2005, A&A, submitted
Vreeswijk, P., et al. 2004, A&A, 419, 927
Wang, J., Hall, P. B., Ge, J., Li, A., & Schneider, D. 2004, ApJ, 609, 589
Webster, R. L., Francis, P. J., Peterson, B. A., Drinkwater, M. J., & Masci, F. J. 1995, Nature, 375, 469
White, R. L., Helfand, D. J., Becker, R. H., Gregg, M. D., Postman, M., Lauer, T. R., & Oegerle, W. 2003, AJ, 126, 706
Whiting, M., Webster, R., & Francis, P. 2001, MNRAS, 323, 718
Wild, V., & Hewett, P. C. 2005, MNRAS, 361, L30
Wucknitz, O., Wisotzki, L., Lopez, S., & Gregg, M. D. 2003, A&A, 405, 445
Zuo, L., Beaver, E. A., Burbidge, E. M., Cohen, R. D., Junkkarinen, V. T., & Lyons, R. W. 1997, ApJ, 477, 568